Ocean-Atmosphere Interaction in the Lifecycle of ENSO: The Coupled Wave Oscillator**

Jialin LIN*

(*Dedicated to Professor Andrew Majda on the Occasion of his* 60*th Birthday*)

Abstract To explain the oscillatory nature of El Nino/Southern Oscillation (ENSO), many ENSO theories emphasize the free oceanic equatorial waves propagating/reflecting within the Pacific Ocean, or the discharge/recharge of Pacific-basin-averaged ocean heat content. ENSO signals in the Indian and Atlantic oceans are often considered as remote response to the Pacific SST anomaly through atmospheric teleconnections. This study investigates the ENSO life cycle near the equator using long-term observational datasets. Space-time spectral analysis is used to identify and isolate the dominant interannual oceanic and atmospheric wave modes associated with ENSO. Nino3 SST anomaly is utilized as the ENSO index, and lag-correlation/regression are used to construct the composite ENSO life cycle. The propagation, structure and feedback mechanisms of the dominant wave modes are studied in detail. The results show that the dominant oceanic equatorial wave modes associated with ENSO are not free waves, but are two ocean-atmosphere coupled waves including a coupled Kelvin wave and a coupled equatorial Rossby (ER) wave. These waves are not confined only to the Pacific Ocean, but are of planetary scale with zonal wavenumbers 1-2, and propagate all the way around the equator in more than three years, leading to the longer than 3-year period of ENSO. When passing the continents, they become uncoupled atmospheric waves. The coupled Kelvin wave has larger variance than the coupled ER wave, making the total signals dominated by eastward propagation. Surface zonal wind stress (x) acts to slow down the waves. The two coupled waves interact with each other through boundary reflection and superposition, and they also interact with an off-equatorial Rossby wave in north Pacific along 15N through boundary reflection and wind stress forcing. The precipitation anomalies of the two coupled waves meet in the eastern Pacific shortly after the SST maximum of ENSO and excite a dry atmospheric Kelvin wave which quickly circles the whole equator and leads to a zonally symmetric signal of troposphere temperature. ENSO signals in the Indian and Atlantic oceans are associated with the two coupled waves as well as the fast atmospheric Kelvin wave. The discharge/recharge of Pacific-basin-averaged ocean heat content is also contributed by the two coupled waves. The above results suggest the presence of an alternative coupled wave oscillator mechanism for the oscillatory nature of ENSO.

Keywords ENSO, Ocean-atmosphere interaction, Equatorial waves
2000 MR Subject Classification 17B40, 17B50

1 Introduction

The El Nino/Southern Oscillation (ENSO) is the dominant interannual mode of the tropical coupled ocean-atmosphere system and a key seasonal-to-interannual predictability of the global climate system (see, e.g., [1]). However, ENSO is not well predicted by the statistical forecast schemes (see, e.g., [2]), nor is it well simulated or predicted by the coupled general circulation models (CGCMs; see, e.g., [3]). There is a large scatter in CGCM-simulated ENSO signals, with most of the models producing an overly short period. This is detrimental to climate prediction of ENSO and its teleconnections, and reflects our limited understanding of the physical mechanisms determining the oscillatory nature of ENSO.

Since the pioneering study of [4], it has been widely accepted that ocean-atmosphere coupling plays a central role in amplifying and maintaining ENSO. The existing ENSO theories have been reviewed comprehensively by many papers (see, e.g., [5, 6]). The theories can be categorized into the following six groups: (1) the slow coupled mode theories, (2) the delayed oscillator theory, (3) the advective-reflective oscillator theory, (4) the western Pacific oscillator theory, (5) the recharge oscillator theory, (6) the stochastic forcing theories. These theories are summarized schematically in Figure 1.
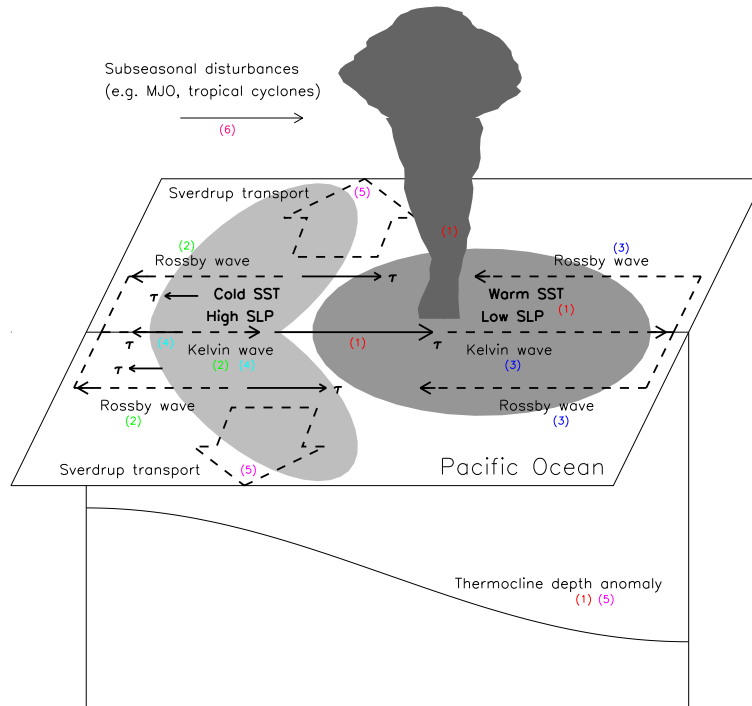

Figure 1 Schematic depiction of the existing ENSO theories. The numbers in color denote that the corresponding process is emphasized by one or more of the existing theories, including (1) the slow coupled mode theory, (2) the delayed oscillator theory, (3) the advective-reflective oscillator theory, (4) the western Pacific oscillator theory, (5) the recharge oscillator theory, and (6) the stochastic forcing theory.

The slow coupled mode theories consider ENSO as a slow coupled ocean-dynamics mode or SST mode (see reviews by [5, 6] and references therein). The simple coupled system (with

constant mean states) displays a slow westward propagating unstable mode and a slow eastward propagating unstable mode, which can propagate and continuously regenerate on interannual timescales, while physical processes in the oceanic surface layer (not related to wave dynamics) can produce a slow SST mode. In most of the parameter space, the coupled modes will have a mixed nature, i.e., the mixed SST/ocean-dynamics modes.

The delayed oscillator theory (see [7, 8]) emphasizes the free upwelling equatorial Rossby (ER) waves forced by the zonal wind stress anomaly in central Pacific associated with El Nino, which propagates westward and is reflected by the western boundary and becomes eastward propagating upwelling Kelvin waves. The returned Kelvin waves kill the warm SST anomaly in the eastern Pacific and initiate cold SST anomaly for a La Nina event, leading to an oscillation.

The advective-reflective oscillator theory (see [9]) emphasizes the free downwelling Kelvin waves forced by the zonal wind stress anomaly in central Pacific associated with El Nino, which propagates eastward and is reflected by the eastern boundary and becomes westward propagating downwelling ER waves. The returned ER waves advect the warm SST anomaly in the eastern Pacific back to western Pacific, and initiate cold SST anomaly in the eastern Pacific for a La Nina event, leading to an oscillation.

The western Pacific oscillator theory (see [10]) emphasizes the free upwelling Kelvin waves forced by the easterly zonal wind stress anomaly in the western Pacific associated with El Nino, which propagates eastward and kill the warm SST anomaly in the eastern Pacific and initiate cold SST anomaly for a La Nina event, leading to an oscillation.

The recharge oscillator theory (see [11, 12]) emphasizes the discharge/recharge of Pacific-ocean-averaged ocean heat content. The restoring force for ENSO comes from the poleward (equatorward) Sverdrup transport associated with wind stress curl (WSC) during the warm (cold) phase, and vertical advection of cold (warm) subsurface temperature anomaly by climatological upwelling during the warm-to-cold (cold-to-warm) transition phase. These lead to a phase difference between the Pacific-basin-averaged OHC anomaly and SST anomaly.

The stochastic forcing theories consider ENSO as a stable mode forced by stochastic forcing, or an unstable mode triggered and/or enhanced by stochastic forcing (see reviews by [5, 6]). The sources of stochastic forcing are tropical intraseasonal modes, such as the Madden-Julian Oscillation, convectively coupled equatorial waves, tropical cyclones, cold surges from midlatitudes, or a combination of them. The stochastic forcing takes the form of surface wind stress and/or surface heat flux. It can be either additive or multiplicative, and some recent modeling studies show that multiplicative forcing has a stronger effect on simulated ENSO mode.

Three of the six ENSO theories, including the delayed oscillator theory, the advective-reflective oscillator theory and the western Pacific oscillator theory, emphasize the free oceanic equatorial waves including the Kelvin wave and the ER wave. A common critique of these theories is that the phase speeds of the free waves are too fast to explain the 4-year period of ENSO. By using satellite sea surface height (SSH) datasets, many studies tried to isolate the free oceanic waves by projecting the observed SSH (or SSH-derived surface currents) onto the theoretical meridional structure of the free waves (see, e.g., [13, 14]). Zonal propagation and reflections at both the western and the eastern boundaries were found, as well as wind forced signals. However, detailed inspection of their figures reveals that the phase speeds of the isolated Kelvin waves and Rossby waves are much slower than those of the theoretical free waves. Actually, it takes about 8–10 months for the observed waves to cross the Pacific Ocean,

which doubles or triples the time expected for free waves. This suggests that the isolated waves may not be free waves, but look more like coupled waves. It is important to note that the method used in these studies for isolating waves, i.e., projection onto theoretical meridional structures of the free waves, does not necessarily give the expected free waves because coupled waves may have similar meridional structures.

The theory of equatorially trapped waves was developed by [15, 16]. The traditional method for identifying and isolating the equatorial waves is space-time spectral analysis (see, e.g., [17]). It has been widely used to study the intraseasonal convectively coupled equatorial waves (see, e.g., [18, 19]). However, to our knowledge, space-time spectral analysis has not been used to study the interannual equatorial waves associated with ENSO.

Moreover, all of the six ENSO theories consider only the equatorial Pacific Ocean. However, highly coherent ENSO signals have been observed outside the Pacific in both the Indian Ocean and the Atlantic Ocean (see [20]). They are often considered as remote response to the Pacific SST anomaly through atmospheric teleconnection mechanisms. However, propagation of ENSO signals from the Indian Ocean to the Pacific Ocean has been observed both along the equator (see, e.g., [21, 22]), and along the northern hemisphere Inter-Tropical Convergence Zone (ITCZ). Therefore, the relation between ENSO signals outside the Pacific basin and those within the Pacific basin is still not clear.

The purpose of this study is to investigate the ENSO life cycle near the equator using long-term observational datasets. Contrasting to the previous studies, the dominant oceanic and atmospheric wave modes associated with ENSO are identified and isolated not by projection onto the meridional structure of theoretical free waves, but by the traditional method of space-time spectral analysis (see, e.g., [17–19]). Nino3 SST is utilized as the ENSO index, and composite life cycle of ENSO is constructed by using lagged correlation/regression with respect to the ENSO index. The questions that we address are: (1) What are the dominant interannual oceanic and atmospheric equatorial wave modes associated with ENSO? (2) What determines the longer than 3-year period of ENSO? (3) What is the relation between ENSO signals in Indian and Atlantic Oceans and those in the Pacific Ocean? (4) What is the relation between the dominant wave modes and the variation of Pacific-basin-averaged ocean heat content?

The observational datasets used in this study and the analysis methods are described in Section 2. The dominant oceanic and atmospheric equatorial wave modes associated with ENSO are analyzed in Section 3. A summary and discussion are given in Section 4.

2 Data and Methods

The long-term monthly observational datasets used in this study are listed in Table 1 together with the acronyms of the variables. For each variable, different datasets are used in order to bracket the uncertainties associated with measurement/retrieval/analysis. Because we are interested only in the large-scale features, unless otherwise specified, all datasets are averaged to have a zonal resolution of 10 degree longitude, while the original meridional resolution are kept. All time series are processed after the following steps. (1) The linear trend is removed. (2) The composite seasonal cycle is removed. (3) Any remained intraseasonal variability is removed by using a 3-month running mean. (4) The dominant interannual wave modes are identified and isolated by using space-time spectral analysis following the method of [18, 19].

The detailed procedure is described in the Appendix. (5) The Nino3 SST anomaly is used as the ENSO index, and the composite ENSO life cycle is constructed by calculating lagged correlation/regression between the ENSO index and the interannual anomaly of any variable, with the statistical significance of lagged correlation assessed following the method of [23].

3 Dominant Equatorial Wave Modes Associated with ENSO

3.1 Space-time spectral analysis

First we use space-time spectral analysis to examine the dominant interannual equatorial wave modes behind the zonally propagating signals associated with ENSO. Figure 2 shows the wavenumber-frequency spectra of 8N-8S averaged (a) Ts, (b) OHC, (c) precipitation, (d) troposphere temperature, (e) Z_{200}, (f) SLP, (g) u_{200}, and (h) τ_x. There are three important conclusions that can be drawn from Figure 2. First, without exception, the spectra of all variables are dominated by two modes: an eastward propagating mode with zonal wavenumbers
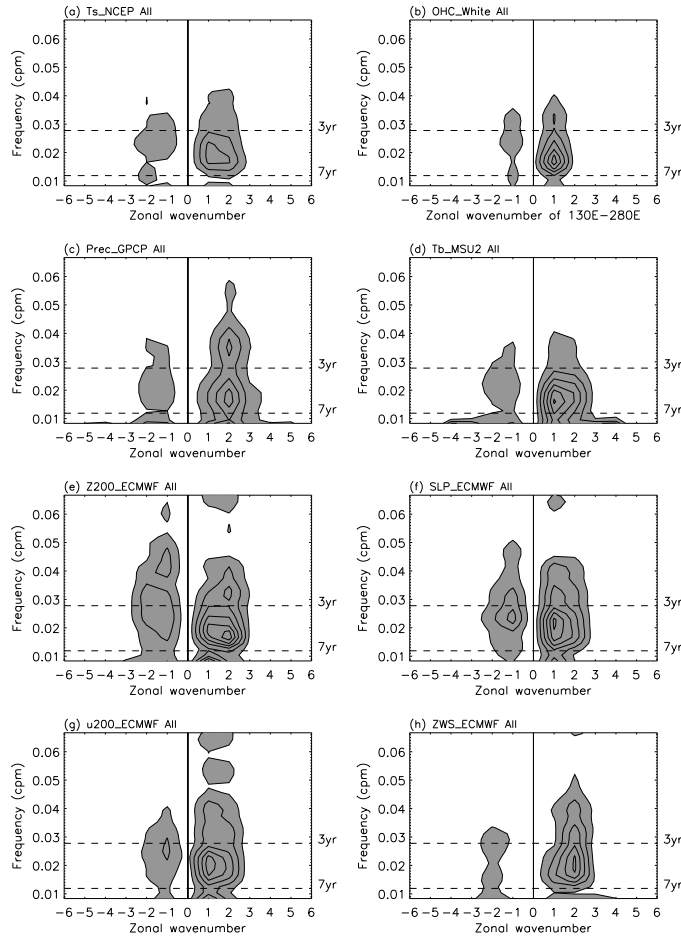

Figure 2　Zonal wavenumber-frequency spectra of the 8N-8S symmetric component of (a) Ts from NCEP reanalysis, (b) OHC, (c) precipitation from GPCP, (d) troposphere temperature for MSU channel 2, (e) Z_{200} from ERA-40, (f) SLP from ERA-40, (g) u_{200} from ERA-40, and (h) τ_x from ERA-40.

1–2 and period 3–7 years, and a westward propagating mode with zonal wavenumbers 1–2 and period 3–7 years. The variance of the eastward mode does not fall along the theoretical Kelvin wave dispersion curves, but falls along a constant wavenumber. The westward mode does not fall along the ER wave dispersion curves either, but also along a constant wavenumber. This reminds us of the behavior of MJO on the intraseasonal wavenumber-frequency spectra, which does not fall along any theoretical equatorial wave dispersion curves, but along a constant frequency (see [18]). Second, for all variables, the variance of the eastward mode is much larger than that of the westward mode, consistent with the dominance of eastward signals in the zonally asymmetric component of all variables (not shown). Third, the phase speed of the two modes is about 0.1–0.3 m/s, which is much smaller than those of the free oceanic equatorial waves, suggesting that they are ocean-atmosphere coupled waves.

The characteristics of the two dominant modes in the time-longitude domain, and for each latitude, can be extracted from the total field by filtering in the wavenumber-frequency domain and then conducting inverse Fourier transform. In this study, the eastward (westward) propagating mode is simply defined to include all eastward (westward) wavenumbers and all frequencies. Since the two modes both correspond to prominent spectral peak, the resultant time series are dominated by signals with zonal wavenumbers 1–2 and period 3–7 years, as will be shown shortly in Subsections 3.2 and 3.3.

3.2 Phase relationships in the coupled Kelvin wave

Next we examine in detail the phase relationships in the coupled Kelvin wave. Figure 3 shows the composite life cycle of the eastward component of (a) NCEP Ts, (b) OHC, (c) GPCP precipitation, (d) MSU channel 2 troposphere temperature, (e) ERA-40 Z_{200}, (f) ERA-40 SLP, (g) ERA-40 u_{200}, and (h) ERA-40 τ_x. The Ts anomaly (see Figure 3(a)) is dominated by a zonal wavenumber-1 signal which propagates all the way around the equator (denoted by the thick solid line in Figure 3(a)). The phase speed displays two distinct regions: a slow region over the Pacific and Atlantic Oceans with a phase speed of about 0.2 degree/day (or 0.25 m/s), and a very fast region over Africa and Indian Ocean (seen more clearly for the negative anomaly near lag 0). The Ts anomaly in the slow region is associated with coherent anomalies in almost all other variables (see Figure 3(b)–(h)), suggesting that it is a coupled wave, while that in the fast region is accompanied by coherent anomalies in troposphere temperature (see Figure 3(d)), Z_{200} (see Figure 3(e)), and SLP (see Figure 3(f)), but not in OHC (see Figure 3(b)), precipitation (see Figure 3(c)) or τ_x (see Figure 3(h)), suggesting that it is a (dry) uncoupled atmospheric wave. There is another Ts signal which starts from the western Indian Ocean and propagates slowly to the western Pacific (denoted by the thick dashed line in Figure 3(a)), where it merges into the slow signal in western Pacific. Similar to the Ts anomaly in the Pacific and Atlantic Oceans, this signal in the Indian Ocean is also accompanied by coherent anomalies in almost all other variables (see Figure 3(b)–(h)), suggesting that it is also part of the coupled Kelvin wave. As will be shown in Subsection 3.4, the initiation of the coupled Kelvin wave in the western Indian Ocean is associated with boundary reflection of the coupled ER wave.

The coupled Kelvin wave displays interesting phase relationships, which are important for understanding the ocean-atmosphere feedback mechanism in the wave. To help examining the phase relationships, we over-plot in all panels the thick solid and dashed lines denoting the phase propagation of SST anomaly. In the coupled Kelvin wave, OHC (see Figure 3(b)) is
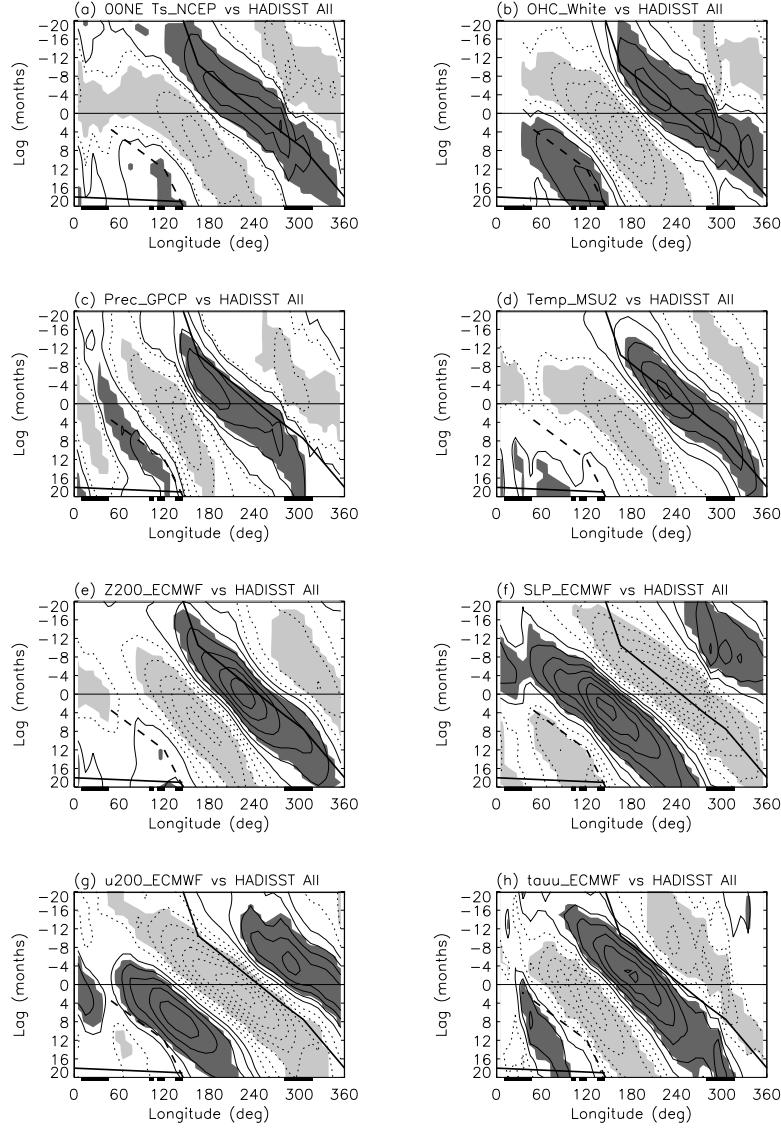
Figure 3 Lag-regression with respect to Nino3 SST anomaly for 8N-8S averaged eastward propagating component of (a) NCEP Ts, (b) OHC, (c) GCCP precipitation, (d) MSU channel 2 temperature, (e) Z_{200}, (f) SLP, (g) u_{200}, and (h) τ_x. The thick solid line and thick dashed line denote the phase propagation of the positive anomaly of NCEP Ts.

nearly in phase with SST, precipitation (see Figure 3(c)) lags SST by about $\frac{1}{8}$ cycle, troposphere temperature (see Figure 3(d)) is nearly in phase with SST, Z_{200} (see Figure 3(e)) lags SST by $\frac{1}{8}$ cycle, SLP (Figure 3(f)) is out of phase with SST, u_{200} (see Figure 3(g)) leads SST by about $\frac{5}{8}$ cycle, and τ_x (see Figure 3(h)) lags SST by a quarter cycle. These phase relationships will be summarized schematically later in Figure 6. Because τ_x (see Figure 3(h)) lags OHC (see Figure 3(b)) by about a quarter cycle, and in oceanic Kelvin wave zonal current is nearly in phase with OHC, τ_x lags the zonal current by about a quarter cycle. This means that τ_x tends to force a westerly zonal current anomaly to the west of the eastward propagating westerly zonal current

anomaly, which just counteracts the effect of the oceanic pressure gradient force. Therefore, τ_x acts to slow down the coupled Kelvin wave.

To summarize, the coupled Kelvin wave propagates all the way around the equator in more than three years, which contributes to the longer than 3-year period of ENSO. When passing the continents, it becomes an uncoupled atmospheric wave. τ_x acts to slow down the wave.

3.3 Phase relationships in the coupled ER wave

Figure 4 is the same as Figure 3 but for the westward propagating component. Similar to the eastward propagating component, the westward propagating component also displays strong correlation with Nino3 SST anomaly, which is useful for statistical prediction and will be discussed later in Section 5.
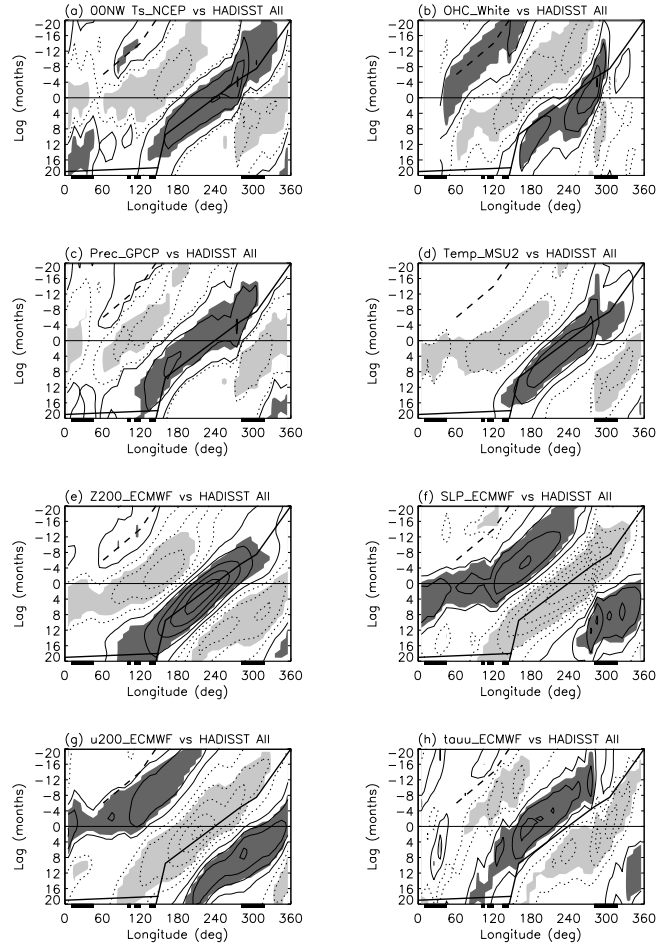

Figure 4 Same as Figure 3 but for the westward propagating component.

The Ts anomaly (see Figure 4(a)) is dominated by a zonal wavenumber-1 signal which propagates all the way around the equator (denoted by the thick solid line in Figure 4(a)). The phase speed displays two distinct regions: a slow region over the Pacific and Atlantic Oceans with a phase speed of about 0.2 degree/day (or 0.25 m/s), and a very fast region over Africa and Indian Ocean (seen more clearly for the negative anomaly near lag 0). The Ts anomaly in

the slow region is associated with coherent anomalies in almost all other variables (see Figure 4(b)–(h)), suggesting that it is a coupled wave, while that in the fast region is accompanied by coherent anomalies in troposphere temperature (see Figure 4(d)), Z_{200} (see Figure 4(e)), and SLP (see Figure 4(f)), but not in OHC (see Figure 4(b)), precipitation (see Figure 4(c)) or τ_x (see Figure 4(h)), suggesting that it is a (dry) uncoupled atmospheric wave. There is another Ts signal which starts from the western Pacific and propagates slowly westward to the western Indian Ocean (denoted by the thick dashed line in Figure 4(a)). Similar to the Ts anomaly in the Pacific and Atlantic Oceans, this signal in the Indian Ocean is also accompanied by coherent anomalies in almost all other variables (see Figure 4(b)–(h)), suggesting that it is also part of the coupled ER wave.

The phase relationships in the coupled ER wave are important for understanding its ocean-atmosphere feedback mechanism. OHC (see Figure 4(b)) lags the SST by about $\frac{1}{8}$ cycle, precipitation (see Figure 4(c)) leads SST by about $\frac{1}{8}$ cycle, troposphere temperature (see Figure 4(d)) slightly lags SST, Z_{200} (see Figure 4(e)) is nearly in phase with SST, SLP (see Figure 4(f)) is out of phase with SST, u_{200} (see Figure 4(g)) leads SST by about $\frac{5}{8}$ cycle, and τ_x (see Figure 4(h)) lags SST by a quarter cycle. These phase relationships will be summarized schematically later in Figure 6. Because τ_x (see Figure 4(h)) leads OHC (see Figure 4(b)) by about $\frac{3}{8}$ cycle, and in oceanic ER wave zonal current is nearly out of phase with OHC, τ_x lags the zonal current by about $\frac{1}{8}$ cycle. This means that τ_x tends to enhance the existing zonal current anomaly, and also force a westerly zonal current anomaly to the east of the westward propagating westerly zonal current anomaly, which just counteracts the effect of the oceanic pressure gradient force. Therefore τ_x acts to amplify and slow down the coupled ER wave.

In summary, the coupled ER wave propagates all the way around the equator in more than three years, which contributes to the longer than 3-year period of ENSO. When passing the continents, it becomes an uncoupled atmospheric wave. τ_x acts to amplify and slow down the wave.

3.4 Interactions between the coupled Kelvin wave and the coupled ER wave

To examine the interaction between the coupled Kelvin wave and the coupled ER wave, Figure 5 shows the composite life cycle of 8N-8S (a) eastward (Kelvin) component of OHC (repetition of Figure 3(b)), and (b) westward (ER) component of OHC (repetition of Figure 4(b)). Comparison between Figure 5(a) and Figure 5(b) suggests boundary reflection at the western boundary of Indian Ocean (denoted by A in the figures), the western boundary of Pacific Ocean (denoted by B), and the eastern boundary of Pacific Ocean (denoted by C). It is important to note that since the two waves are both coupled waves, boundary reflection is not the necessary condition for exciting or maintaining any of them, but only acts to enhance or weaken the waves.

Previous observational studies have demonstrated that the equatorial ENSO OHC signal also interacts with an off-equatorial Rossby wave in the northern Pacific along 15N through boundary reflection (see, e.g., [24]). To illustrate this interaction, Figure 5 also shows (c) 260E-280E averaged OHC, (d) 260E-280E averaged WSC, (e) 10N-20N averaged OHC, and (f) 120E-140E averaged OHC. At the eastern boundary of Pacific Ocean (see Figure 5(c)), there is a poleward phase propagation (reflection) in both the northern and the southern hemispheres, together with a WSC forcing in the northern hemisphere (see Figure 5(d)). The boundary

reflection and the WSC forcing together drive a westward propagating off-equatorial Rossby wave between 10N and 20N which reaches the western boundary of Pacific Ocean in nearly two years (see Figure 5(e)) and is reflected back at the western boundary (equatorward phase propagation) to contribute to the Kelvin wave (see Figure 5(f)). This corroborates the results of many previous studies and further demonstrates that, in addition to boundary reflection, WSC forcing may also play a role in exciting the off-equatorial Rossby wave at the eastern boundary.
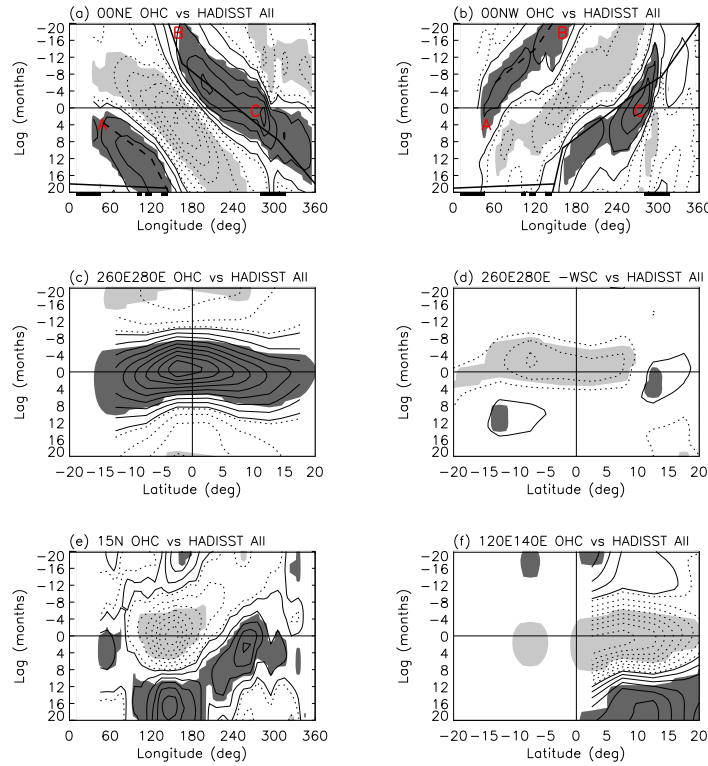
Figure 5 Same as Figure 3 but for (a) 8N-8S averaged eastward propagating component of OHC, (b) 8N-8S averaged westward propagating component of OHC, (c) 260E-280E averaged OHC, (d) 260E-280E averaged WSC, (e) 10N-20N averaged OHC, and (f) 120E-140E averaged OHC.

In short, the coupled Kelvin and ER waves interact with each other through boundary reflection at the western boundary of Indian Ocean and both the western and the eastward boundaries of Pacific Ocean, and they also interact with an off-equatorial Rossby wave in north Pacific along 15N through both boundary reflection and wind stress forcing. The precipitation anomalies of the two waves meet in the eastern Pacific during the mature phase of ENSO, which excite the very fast dry atmospheric Kelvin wave leading to the zonally symmetric component of troposphere temperature.

4 Summary and Discussion

Figure 6 summarizes schematically the results of this study. As discussed in the introduction, three of the six ENSO theories emphasize the role of free oceanic equatorial waves, and all of
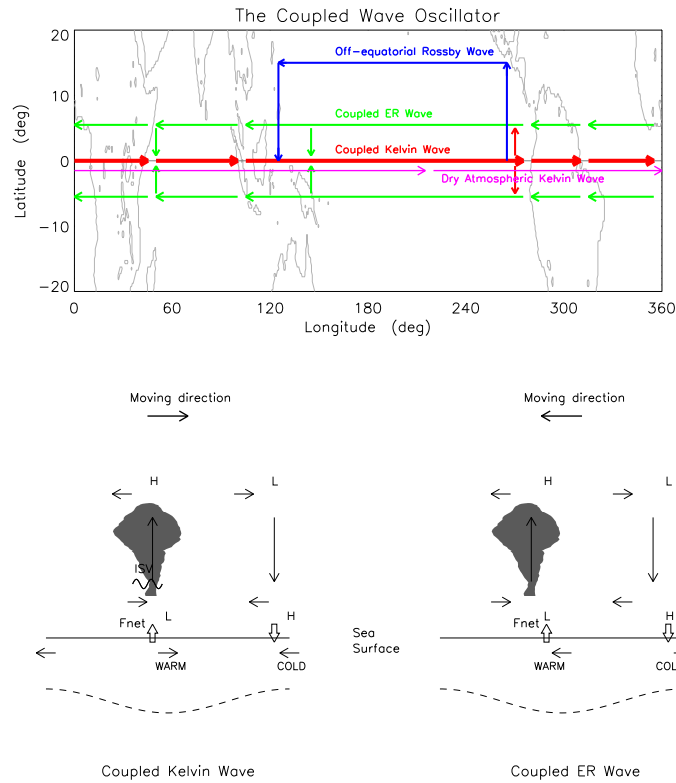
Figure 6 Schematic depiction of the coupled wave oscillator. The upper panel shows the propagation characteristics of the waves. The lower panels show the phase relationships in the coupled Kelvin wave (left) and the coupled ER wave (right). The clouds represent the atmospheric diabatic heating. The arrows represent atmospheric circulation and ocean currents. H and L represent high and low geopotential height anomalies, respectively. WARM and COLD represent SST anomalies. The dashed line represents thermocline depth anomaly.

the six ENSO theories consider only the equatorial Pacific Ocean. However, our results show that the dominant oceanic equatorial wave modes associated with ENSO are not free waves, but are two coupled waves including a coupled Kelvin wave and a coupled ER wave. Moreover, these waves are not confined only to the Pacific Ocean, but are of planetary scale with zonal wavenumbers 1-2, and propagate all the way around the equator in more than three years, leading to the longer than 3-year period of ENSO. When passing the continents, they become uncoupled atmospheric waves. The coupled Kelvin wave has larger variance than the coupled ER wave, making the total signals dominated by eastward propagation. Surface zonal wind stress acts to slow down the waves. The two coupled waves interact with each other through boundary reflection and superposition, and they also interact with an off-equatorial Rossby wave in north Pacific along 15N through boundary reflection and wind stress forcing. The precipitation anomalies of the two coupled waves meet in the eastern Pacific shortly after the SST maximum of ENSO and excite a dry atmospheric Kelvin wave which quickly circles the whole equator and leads to a zonally symmetric signal of troposphere temperature. The recharge oscillator theory of ENSO emphasizes the discharge/recharge of Pacific-basin-averaged ocean heat content. Our results support the existence of this discharge/recharge process and show

that it is also contributed by the two coupled waves. The above results suggest the presence of an alternative coupled wave oscillator mechanism for the oscillatory nature of ENSO.

Figure 6 also summarizes the wave structure along the equator for the coupled Kelvin and ER waves. In the coupled Kelvin wave, OHC (and inferred surface zonal current) is nearly in phase with SST, precipitation lags SST by about $\frac{1}{8}$ cycle, troposphere temperature is nearly in phase with SST, Z_{200} lags SST by $\frac{1}{8}$ cycle, SLP is out of phase with SST, u_{200} leads SST by about $\frac{5}{8}$ cycle, and τ_x lags SST by a quarter cycle. Because τ_x lags the inferred zonal current by about a quarter cycle, τ_x tends to force a westerly zonal current anomaly to the west of the eastward propagating westerly zonal current anomaly, which just counteracts the effect of the oceanic pressure gradient force. Therefore, τ_x acts to slow down the coupled Kelvin wave.

In the coupled ER wave, OHC lags the SST by about $\frac{1}{8}$ cycle, precipitation leads SST by about $\frac{1}{8}$ cycle, troposphere temperature slightly lags SST, Z_{200} is nearly in phase with SST, SLP is out of phase with SST, u_{200} leads SST by about $\frac{5}{8}$ cycle, and τ_x lags SST by a quarter cycle. Since τ_x lags the inferred zonal current by about $\frac{1}{8}$ cycle, τ_x tends to enhance the existing zonal current anomaly, and also force a westerly zonal current anomaly to the east of the westward propagating westerly zonal current anomaly, which just counteracts the effect of the oceanic pressure gradient force. Therefore, τ_x acts to amplify and slow down the coupled ER wave.

Our results may help to understand and alleviate CGCMs biases in their ENSO simulations. Currently, we are evaluating the life cycle of ENSO in 22 IPCC AR4 coupled GCMs, and the preliminary results show that the too short ENSO periods in many models are associated with too fast phase speeds of the coupled equatorial waves. We are analyzing the ocean-atmosphere feedbacks and the relationship with OGCMs mean state (see, e.g., [25, 26]). The results will be reported in a separate study.

Table 1 Datasets used in this study

Variable (Acronym)	Dataset	Spatial Coverage Resolution (deg)	Temporal Coverage	Reference
Surface skin temperature (Ts)	NCEP reanalysis	Global 2.5×2.5	1960–1999	[27]
Ocean heat content (OHC)	Scripps ocean analysis	Global ocean 5×2	1960–1999	[28]
Precipitation	GPCP	Global 2.5×2.5	1979–2004	[29]
Troposphere temperature	MSU channel 2	Global 2.5×2.5	1979–2004	[30]
200mb geopotential height (Z_{200})	NCEP reanalysis	Global 2.5×2.5	1960–1999	[27]
200mb zonal wind (u_{200}) 200mb meridional wind (v_{200}) sea level pressure (SLP) surface zonal wind stress (τ_x) surface wind stress curl (WSC)	ERA-40 reanalysis	Global 2.5×2.5	1960–1999	[31]

References

[1] Philander, S. G., El Niño, La Niña, and the Southern Oscillation, Academic Press, London, 1990.

[2] Barnston, A. G., He, Y. and Glantz, M. H., Predictive skill of statistical and dynamical climate models in SST forecasts during the 1997–1998 El Niño episode and the 1998 La Niña onset, *Bull. Amer. Meteor. Soc.*, **80**, 1999, 217–244.

[3] Lin, J. L., Interdecadal variability of ENSO in 21 IPCC AR4 coupled GCMs, *Geophys. Res. Let.*, **34**, 2007, L12702. DOI:10.1029/2006GL028937

[4] Bjerknes, J., Atmospheric teleconnections from the equatorial Pacific, *Mon. Weather Rev.*, **97**, 1969, 163–172.

[5] Neelin, J. D., Battisti, D. S., Hirst, A. C., et al, ENSO theory, *J. Geophys. Res.*, **103**, 1998, 14261–14290.

[6] Wang, C. and Picaut, J., Understanding ENSO physics — A review, Earth's Climate: The Ocean-Atmosphere Interaction, C. Wang, S.-P. Xie and J. A. Carton (eds.), AGU Geophysical Monograph Series, **147**, 2004, 21–48.

[7] Suarez, M. J. and Schopf, P. S., A delayed action oscillator for ENSO, *J. Atmos. Sci.*, **45**, 1988, 3283–3287.

[8] Battisti, D. S. and Hirst, A. C., Interannual variability in the tropical atmosphere-ocean model: influence of the basic state, ocean geometry and nonlineary, *J. Atmos. Sci.*, **46**, 1989, 1687–1712.

[9] Picaut, J., Masia, F. and du Penhoat, Y., An advective-reflective conceptual model for the oscillatory nature of the ENSO, *Science*, **277**, 1997, 663–666.

[10] Weisberg, R. H. and Wang, C., A western Pacific oscillator paradigm for the El Niño-Southern Oscillation, Geophys, *Res. Lett.*, **24**, 1997, 779–782.

[11] Jin, F.-F., An equatorial ocean recharge paradigm for ENSO, Part I: Conceptual model, *J. Atmos. Sci.*, **54**, 1997, 811–829.

[12] Jin, F.-F., An Equatorial ocean recharge paradigm for ENSO, Part II: a stripped-down coupled model, *J. Atmos. Sci.*, **54**, 1997, 830–847.

[13] Boulanger, J.-P. and Menkes, C., Propagation and reflection of long equatorial waves in the Pacific ocean during the 1992–1993 El Niño, *J. Geophys. Res.*, **100**, 1995, 25041–25059.

[14] Picaut, J., Hackert, E., Busalacchi, A. J., et al, Mechanisms of the 1997–1998 El Niño-La Niña, as inferred from space-based observations, *J. Geophys. Res.*, **107**, 2002, 30–37. DOI:10.1029/2001JC000850

[15] Matsuno, T., Quasi-geostrophic motions in the equatorial area, *J. Meteor. Soc. Japan*, **44**, 1966, 25–43.

[16] Lindzen, R. S., Planetary waves on beta-planes, *Mon. Wea. Rev.*, **95**, 1967, 441–451.

[17] Hayashi, Y., Space-time spectral analysis and its applications to atmospheric waves, *J. Meteor. Soc. Japan*, **60**, 1982, 156–171.

[18] Wheeler, M. and Kiladis, G. N., Convectively coupled equatorial waves: analysis of clouds and temperature in the wavenumber-frequency domain, *J. Atmos. Sci.*, **56**, 1999, 374–399.

[19] Lin, J. L., Kiladis, G. N., Mapes, B. E., et al, Tropical intraseasonal variability in 14 IPCC AR4 climate models, Part I: Convective signals, *J. Climate*, **19**, 2006, 2665–2690.

[20] Alexander, M. A., Blade, I., Newman, M., et al, The atmospheric bridge: The influence of ENSO teleconnections on airsea interaction over the global oceans, *J. Climate*, **15**, 2002, 2205–2231.

[21] Barnett, T. P., Interaction of the Monsoon and Pacific trade wind system at interannual time scales, Part I: The equatorial zone, *Mon. Wea. Rev.*, **111**, 1983, 756–773.

[22] Trenberth, K. E., Caron, J. M., Stepaniak, D. P., et al, Evolution of El Niño-Southern Oscillation and global atmospheric surface temperatures, *J. Geophys. Res.*, **107**, 2002, 40–65. DOI:10.1029/2000JD000298

[23] Oort, A. H. and Yienger, J. J., Observed long-term variability in the Hadley circulation and its connection to ENSO, *J. Climate*, **9**, 1996, 2751–2767.

[24] White, W. B., Tourre, Y. M., Barlow, M., et al, A delayed action oscillator shared by biennal, interannual, and decadal signals in the Pacific basin, *J. Geophys. Res.*, **108**, 2003, 30–70. DOI:10.1029/2002JC001490

[25] Lin, J. L., The double-ITCZ problem in IPCC AR4 coupled GCMs: Ocean-atmosphere feedback analysis, *J. Climate*, **20**, 2007, 4497–4525.

[26] Lin, J. L., Mapes, B. E. and Han, W., What are the sources of mechanical damping in Matsuno-Gill type models? *J. Climate*, **21**, 2008, 165–179.

[27] Kalnay, E., Kanamitsu, M., Kistler, R., et al, The NCEP/NCAR 40-Year Reanalysis Project, *Bull. Amer. Meteor. Soc.*, **77**, 1996, 437–471.

[28] White, W. B., Design of a global observing system for gyre-scale upper ocean temperature variability, *Prog. Oceanogr.*, **36**, 1995, 169–217.

[29] Adler, R. F., Huffman, G. J., Chang, A., et al, The version 2 global precipitation climatology project (GPCP) monthly precipitation analysis (1979–present), *J. Hydrometeor.*, **4**, 2003, 1147–1167.

[30] Christy, J. R., Spencer, R. W., Norris, W. B., et al, Error estimates of version 5.0 of MSU-AMSU bulk atmospheric temperatures, *J. Atmos. Oceanic Technol.*, **20**, 2003, 613–629.

[31] Gibson, J. K., Kllberg, P., Uppala, S., et al, ERA description, ECMWF Reanalysis Project Report, Ser. 1, 1997.